

Modeling of CH₄-assisted SOEC for H₂O/CO₂ co-electrolysis

Haoran Xu^a, Bin Chen^a, John Irvine^b, Meng Ni^{a*}

^aBuilding Energy Research Group, Department of Building and Real Estate

The Hong Kong Polytechnic University, Hung Hom, Kowloon, Hong Kong, China

^b School of Chemistry, University of St Andrews, St Andrews, Fife, KY16 9ST, UK

Abstract:

Co-electrolysis of H₂O and CO₂ in a solid oxide electrolysis cell (SOEC) is promising for simultaneous energy storage and CO₂ utilization. Fuel-assisted H₂O electrolysis by SOEC (SOFEC) has been demonstrated to be effective in reducing power consumption. In this paper, the effects of fuel (i.e. CH₄) assisting on CO₂/H₂O co-electrolysis are numerically studied using a 2D model. The model is validated with the experimental data for CO₂/H₂O co-electrolysis. One important finding is that the CH₄ assisting is effective in lowering the equilibrium potential of SOEC thus greatly reduces the electrical power consumption for H₂O/CO₂ co-electrolysis. The performance of CH₄-assisted SOFEC increases substantially with increasing temperature, due to increased reaction kinetics of electrochemical reactions and CH₄ reforming reaction. The CH₄-assisted SOFEC can generate electrical power and syngas simultaneously at a low current density of less than 600Am⁻² and at 1123K. In addition, different from conventional SOEC whose performance weakly depends on the anode gas flow rate, the CH₄-assisted SOFEC performance is sensitive to the anode gas flow rate (i.g. peak current density is achieved at an anode flow rate of 70 SCCM at 1073K). The model can be used for subsequent design optimization of SOFEC to achieve high performance energy storage.

Keywords: Solid oxide electrolyzer cell; Mathematical modeling; Fuel assisting; Co-electrolysis; Cogeneration; Solid oxide fuel cell

* Corresponding author

Email: bsmengni@polyu.edu.hk; Tel: 852-27664152; Fax: 852-27645131

1. Introduction

Clean and sustainable energy technologies are urgently needed to address the fossil fuels-related energy crisis and environmental problems such as global warming, air pollution and acid rain. Renewable energies like solar energy and wind energy can hopefully meet our requirements. However, they are restricted in time and space and not reliable for instantaneous supply of energy [4]. Therefore, effective energy storage is critical for renewable energy applications. Solid oxide electrolysis cell (SOEC) is a high temperature electrochemical cell suitable for converting excess renewable power to fuels [5]. The produced fuel can be later converted back into electrical power via fuel cells when the renewable power is insufficient. Compared with low temperature electrolyzers, the electrical energy requirement of SOEC is relatively low as a significant part of energy input to SOEC is heat [1]. In addition, the high operating temperature of SOEC enables the use of non-noble metal catalyst, leading to lower cost of the system. SOECs are capable of co-electrolyzing CO₂ and H₂O to produce syngas (H₂ and CO mixture), which can be further processed for gaseous or liquid fuel generation using Fischer-Tropsch (F-T) reactor [6-13]. Becker et al.[9] developed a model for high temperature SOEC co-electrolysis for syngas production and subsequent conversion to liquid fuels by F-T process. They also evaluated the economics of production plant considering variations in electricity feedstock costs and operating capacity factors. Stempien et al.[12] further analyzed the thermodynamics of the combined SOEC and F-T processes. They proposed an optimized system that achieved overall efficiency of 66.67%. Chen et al.[13] integrated the high-temperature CO₂-H₂O co-electrolysis and low temperature F-T synthesis in a single tubular unit and reached 11.40% of CH₄ yield with an overall CO₂ conversion ratio of 64.1%. Chen et al.[10] modeled this one-step system and identified optimal operating conditions. The combination of SOEC co-electrolysis and F-T process offers an alternative way of utilizing the captured CO₂ for fuel synthesis using excessive renewable power.

For widespread application of SOEC, its electrical energy consumption needs to be further reduced as the quality of electricity (i.e. exergy) is high. Recent studies have demonstrated that by supplying low cost fuel to the anode of SOEC (termed as fuel-assisted SOEC) for steam electrolysis could significantly reduce the operating potential of SOEC thus greatly reduce the electrical power consumption[14]. Despite of preliminary modeling study on fuel-assisted SOEC for H₂O electrolysis, the current literature is lacking detailed modeling of fuel-assisted SOEC for syngas production by CO₂/H₂O co-electrolysis which is very different from steam electrolysis due to the more complicated reaction processes.

To fill the research gap, a 2D mathematical model is developed for an axisymmetric-tubular CH₄-assisted SOFEC (CH₄-SOFEC) for H₂O/CO₂ co-electrolysis. For SOECs exposed to more than one gas, oxygen partial pressure model is adopted as suggested by Stempien et al.[15] The model is validated with the experimental data for CO₂/H₂O co-electrolysis. Parametric simulations are conducted to understand the effect of fuel assisting on the performance of SOEC and the interplay of different physical/chemical processes.

2. Model development

2.1. Model assumption and calculation domain

The 2D numerical model of tubular SOEC is developed by coupling governing equations of electrochemical reaction, chemical reactions, ionic/electronic charge transport, mass transport and momentum transport. In the literature, Luo et al.'s work[16] on syngas production by co-electrolysis provides detailed experimental setup and operating conditions, such as the cathode inlet gas composition, the operation temperature, the thickness of SOEC components, etc. In their study, the current-voltage (I-V) characteristics of CO₂/H₂O co-electrolysis by a cathode supported tubular SOEC are measured.

The working process and modeling geometry of the tubular SOEC unit are shown in Fig. 1.

Steam, carbon dioxide and H₂ are supplied to the cathode channel with length 70mm, inner diameter 3mm and outer diameter 5mm. Air is supplied to the anode channel with length 70mm and outer diameter 10.09mm. The thickness of cathode support layer, cathode active layer, electrolyte and anode are 760μm, 10μm, 10μm and 15μm, respectively. In addition, the modeled tubular SOEC uses porous Ni-YSZ (the mixture of nickel and YSZ (yttrium stabilized zirconium)) as cathode support layer, porous Ni-ScSZ (the mixture of nickel and ScSZ (Scandium stabilized zirconium)) as cathode active layer, dense ScSZ as electrolyte and porous LSM-ScSZ (the mixture of LSM (lanthanum strontium manganate) and ScSZ) as anode. The current is measured at operating potentials from 0.9 V to 1.4 V.

The working process and modeling geometry of the methane-assisted tubular SOFEC unit are shown in Fig. 2. CH₄ and H₂O are supplied to the anode channel with length 70mm, inner diameter 3mm and outer diameter 5mm. Steam and carbon dioxide are supplied to the cathode channel with length 70mm and outer diameter 10.09mm. The thickness of cathode support layer, cathode active layer, electrolyte and anode are 760μm, 10μm, 10μm and 15μm, respectively. In addition, the modeled tubular SOEC uses Ni-YSZ (the mixture of nickel and YSZ (yttrium stabilized zirconium)) as anode support layer, Ni-ScSZ (the mixture of nickel and ScSZ (Scandium stabilized zirconium)) as cathode active layer, ScSZ as electrolyte and Ni-ScSZ as cathode. The material properties of CH₄-SOFEC are assumed to be the same with that of SOEC.

The main assumptions are shown as the following.

- (1) The reaction sites are uniformly distributed in the porous electrodes. However, the electrochemical reactions in the porous electrodes are not uniform and limited to a thin layer near the electrode-electrolyte interface.
- (2) The ionic and electronic charge transport processes take place in PEN (Positive Electrode-

Electrolyte-Negative electrode assembly).

(3) All of the gases (CO, CO₂, H₂, H₂O, CH₄ and N₂) are considered as ideal gases. The flow is considered to be incompressible.

(4) Temperature distribution is uniform in the SOEC.

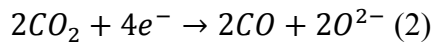
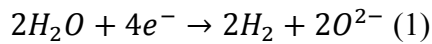
(5) H₂/H₂O and CO/CO₂ are the main reactants in electrochemical reactions.

2.2. Governing equations

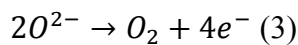
The micro-scale tubular SOEC model couples the process of electrochemical reactions in porous electrodes, chemical reactions in channels and porous electrodes, ionic/electronic charge transport in electrolyte and electrodes, mass transport in channels and micro-pores and momentum transport in channels and micro-pores.

2.2.1. Electrochemical reaction model

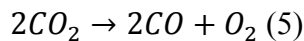
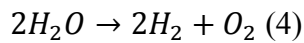
As shown in Fig.1, the gas mixture of H₂O, CO₂, H₂, and CO flows in the cathode channel while the gas mixture of CH₄, O₂, H₂O and CO₂ flows in the anode channel. In the porous cathode, both H₂O and CO₂ molecules diffuse through the porous electrode to the triple-phase-boundary (TPB), where they are reduced to H₂ and CO via reactions (1) and (2), respectively.



The oxygen ions (O²⁻) transport through the dense electrolyte to TPB at anode, where they lose electrons to form oxygen molecules as described in reaction (3).



The overall reactions for H₂O electrolysis and CO₂ electrolysis can be written as:



In operation, the required potential (V) applied to SOEC can be expressed as[17]:

$$V = E + \eta_{act,an} + \eta_{act,ca} + \eta_{ohmic} \quad (6)$$

where E is the equilibrium potential (Nernst potential) related with thermodynamics; η_{act} is the activation overpotentials reflecting the electrochemical activity of the electrodes; η_{ohmic} is the ohmic overpotential influenced by ionic and electronic conduction.

2.2.1.1. Equilibrium potential (Nernst potential)

In SOEC co-electrolysis, the equilibrium potentials for reactions (4) and (5) can be determined by Eqs. (7) and (8), respectively [11]. It should be noted that the concentration overpotentials are included in the equilibrium potential as the gas partial pressure at the reaction sites are used in the calculation.

$$E_{H_2} = E_{H_2}^0 + \frac{RT}{2F} \ln \left[\frac{P_{H_2}^L (P_{O_2}^L)^{1/2}}{P_{H_2O}^L} \right] \quad (7)$$

$$E_{CO} = E_{CO}^0 + \frac{RT}{2F} \ln \left[\frac{P_{CO}^L (P_{O_2}^L)^{1/2}}{P_{CO_2}^L} \right] \quad (8)$$

where E^0 is the voltage under standard conditions (where the pressure of each gas component is 1 atm); R is the universal gas constant ($8.3145 \text{ Jmol}^{-1}\text{K}^{-1}$); T is temperature (K); F is the Faraday constant (96485 Cmol^{-1}) and $P_{H_2}^L$, $P_{H_2O}^L$, P_{CO}^L , $P_{CO_2}^L$ and $P_{O_2}^L$ are the local partial pressures of H_2 , H_2O , CO , CO_2 and O_2 at the TPB (reaction sites), respectively. The value of E^0 between 600K and 1200K for H_2 and CO can be calculated by Eq. (9) and Eq. (10)[6]:

$$E_{H_2}^0 = 1.253 - 0.00024516T \text{ (V)} \quad (9)$$

$$E_{CO}^0 = 1.46713 - 0.0004527T \text{ (V)} \quad (10)$$

Thus, the Nernst potentials can be calculated by combining Eqs. (7) - (10) as:

$$E_{H_2}^0 = 1.253 - 0.00024516T + \frac{RT}{2F} \ln \left[\frac{P_{H_2}^L (P_{O_2}^L)^{1/2}}{P_{H_2O}^L} \right] \text{ (V)} \quad (11)$$

$$E_{CO}^0 = 1.46713 - 0.0004527T + \frac{RT}{2F} \ln \left[\frac{P_{CO}^L (P_{O_2}^L)^{1/2}}{P_{CO_2}^L} \right] \text{ (V)} \quad (12)$$

The Nernst potential calculation is a bit different in methane assisted SOEC co-electrolysis since H₂ and CO are considered as the main reactants in anode electrochemical reactions instead of O₂. The model based on oxygen partial pressure (Eq. 13) is adopted as suggested by Stempien et al.[15].

$$E_{ocv} = \frac{RT}{zF} \ln \left(\frac{\sum P_{O_2,ca}^L}{\sum P_{O_2,an}^L} \right) \quad (13)$$

where E_{ocv} is the open circuit potential, z is the number of electrodes transferred per electrochemical reaction.

For H₂O/H₂ and CO₂/CO system, the oxygen partial pressure can be expressed as shown in Eq. (14) and Eq. (15):

$$P_{O_2,H_2O/H_2}^L = \left(\frac{H_2O^L}{H_2^L} \cdot e^{\frac{\Delta G_{H_2O/H_2}}{RT}} \right)^2 \quad (14)$$

$$P_{O_2,CO_2/CO}^L = \left(\frac{CO_2^L}{CO^L} \cdot e^{\frac{\Delta G_{CO_2/CO}}{RT}} \right)^2 \quad (15)$$

where $\Delta G_{H_2O/H_2}$ is the Gibbs free energy change in the H₂ oxidation reaction and $\Delta G_{CO_2/CO}$ is the Gibbs free energy change in the CO oxidation reaction.

The Nernst potential in CH₄-SOFEK can then be calculated as the difference of cathode and anode partial potential caused by oxygen partial pressure as shown in Eq. (16).

$$E_{th} = \frac{RT}{4F} \ln \frac{P_{O_2}^A}{P_{O_2}^C} \quad (16)$$

2.2.1.2. Activation overpotential

The activation overpotentials are related to the activation energy barrier for electrochemical reactions to proceed. The Butler-Volmer equation is widely used for determining the relationship between the activation overpotential and the current density[18]:

$$i = i_0 \left\{ \exp\left(\frac{\alpha n F \eta_{act}}{RT}\right) - \exp\left(\frac{(1-\alpha)n F \eta_{act}}{RT}\right) \right\} \quad (17)$$

where i_0 is the exchange current density, α is the electronic transfer coefficient and n is the number of electrons transferred per electrochemical reaction. The cathode exchange current density $i_{0,ca}$ for H₂O electrolysis can be expressed as:

$$i_{0,ca,H_2O} = \beta_{H_2} \frac{P_{H_2O}}{P_{ref}} \frac{P_{H_2}}{P_{ref}} \exp\left(-\frac{E_a}{RT}\right) \quad (18)$$

Shi's experimental work has shown that the rate of H₂O electrolysis is about 2.2 times stronger than CO₂ electrolysis, which is also verified in their SOEC co-electrolysis models [16], thus it is assumed that

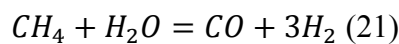
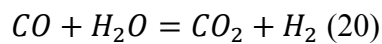
$$i_{0,ca,H_2O} = 2.2 i_{0,ca,CO_2} \quad (19)$$

2.2.1.2. Ohmic overpotential

The ohmic overpotential in a SOEC consists of ionic ohmic overpotential and electronic ohmic overpotential. The ionic and electronic conductivity of electrode and electrolyte materials can be found in Table. 1. The ohmic overpotential can be calculated by the Ohm's law, more detailed calculation can be found in[17].

2.2.2. Chemical reaction model

In the cathode side, reversible water-gas shift reaction (WGSR) and Steam Methane Reforming Reaction (SMR) are considered as the main reactions as shown in Eq. (20) and Eq. (21)[19], respectively.



Due to the excellent catalytic activity of Ni towards the two reactions, LSM-ScSZ is replaced by Ni-ScSZ and the reaction zone is assumed to be limited in the cathode containing Ni catalyst.

The reversible WGSR rate (R_{WGSR} mol m⁻³ s⁻¹) and SMR rate (R_{SMR} mol m⁻³ s⁻¹) can be determined by widely used expressions as:

$$R_{WGSR} = k_{sf}(p_{H_2O}p_{CO} - \frac{p_{H_2}p_{CO_2}}{K_{ps}}) \quad (22)$$

$$k_{sf} = 0.0171 \exp(\frac{-103191}{RT}) \text{ (mol m}^{-3} \text{ Pa}^{-2} \text{ s}^{-1}) \quad (23)$$

$$K_{ps} = \exp(-0.2935Z^3 + 0.6351Z^2 + 4.1788Z + 0.3169) \quad (24)$$

$$Z = \frac{1000}{T} - 1 \quad (25)$$

$$R_{MSR} = k_{rf}(p_{CH_4}p_{H_2O} - \frac{p_{H_2}^3 p_{CO}}{K_{pr}}) \quad (26)$$

$$k_{rf} = 2395 \exp(\frac{-231266}{RT}) \text{ (mol m}^{-3} \text{ Pa}^{-2} \text{ s}^{-1}) \quad (27)$$

$$K_{pr} = 1.0267 \times 10^{10} \exp(-0.2513Z^4 + 0.3665Z^3 + 0.5810Z^2 - 27.134Z + 3.277) \quad (28)$$

In the anode side, H₂ and CO are produced by SMR in porous anode, where WGSR is also considered.

2.2.3. Mass transport model

For the porous electrode, gas diffusion occurs by means of both free molecular diffusion and Knudsen diffusion. Free molecular diffusion dominates in large pores and Knudsen diffusion becomes significant when pore sizes are comparable or smaller than molecular mean-free path.

The extended Fick's model is used to describe gas transport in the porous electrodes as[20]:

$$N_i = -\frac{1}{RT} \left(\frac{B_0 y_i P}{\mu} \frac{\partial P}{\partial z} - D_i^{eff} \frac{\partial (y_i P)}{\partial z} \right) \quad (i = 1, \dots, n) \quad (29)$$

Where N_i represents the flux of mass transport, B_0 is the permeability coefficient, y_i is the mole fraction of component i , μ is the dynamic viscosity of the gas and D_i^{eff} is the effective diffusivity of species i . In an SOEC where both molecular diffusion (D_{im}^{eff}) and Knudsen diffusion (D_{ik}^{eff}) are important, D_i^{eff} can be written as:

$$D_i^{eff} = \left(\frac{1}{D_{im}^{eff}} + \frac{1}{D_{ik}^{eff}} \right)^{-1} \quad (30)$$

D_{im}^{eff} and D_{ik}^{eff} depend on the micro-structure of the porous electrode and operating conditions, the detailed calculation of these two parameters are described in[21, 22].

2.2.4. Momentum conservation model

The general Navier-Stokes equation is used to describe the momentum conservation. For momentum conservation in channels, the equation can be described as:

$$\rho \frac{\partial u}{\partial t} + \rho u \nabla u = -\nabla p + \nabla [\mu (\nabla u + (\nabla u)^T) - \frac{2}{3} \mu \nabla u] \quad (31)$$

For momentum conservation in porous electrodes, the equation is modified by including the Darcy's term for momentum conservation in the porous layer:

$$\rho \frac{\partial u}{\partial t} + \rho u \nabla u = -\nabla p + \nabla [\mu (\nabla u + (\nabla u)^T) - \frac{2}{3} \mu \nabla u] - \frac{\varepsilon \mu u}{k} \quad (32)$$

where ρ is the gas density, u is the velocity vector, p is pressure and ε is the porosity the electrode. More detailed calculation of these parameters can be found in[23].

2.3. Boundary conditions

2.3.1. Electrochemical reaction

The electric potentials are specified at the outer boundaries of anode and cathode as working potential and zero potential, respectively. The bottom and top of the cell is considered to be insulation.

2.3.2. Mass transport

Inflow gas mole fractions are specified at both cathode inlet and anode inlet, for the cathode and anode outlet, the convective flux boundary condition is specified. Zero flux is assumed at the electrolyte/electrode interface and the ends of electrodes.

2.3.4. Momentum conservation

Standard gas flow rate (standard cubic centime per minute: SCCM) is specified at both cathode and anode inlet while pressure condition is specified at the outlet. No slip condition is applied to the electrolyte/electrode interface and the ends of electrodes.

2.4. Model parameters

For model validation, the values material property and operation parameters are consistent with experimental conditions in ref. [10] as shown in Table 1 and Table 2. In parametric simulations, the parameters are varied to evaluate their effects on the SOEC performance. The tuning parameters used for base-case simulation are summarized in Table 3.

2.5. Model solution

The model is solved at certain cell voltage/inlet gas flow rate/inlet gas species mole fraction/temperature. The outputs of the model are the distributions of current density, species concentration, chemical reaction rates and others. The calculations are performed using the finite element commercial software COMSOL MULTIPHYSICS®.

3. Results and discussion

3.1. Model evaluation

In this section, the modeling results of current-voltage characteristics are compared with experimental data for model validation. The model tuning parameters can be found in Table 3. The simulation results and experimental data are compared in Fig. 3. Small difference between the modeling results and experimental data is achieved. In the subsequent parametric simulation, the operation voltage, inlet gas flow rate and inlet gas composition are purposely

varied to evaluate their effects on SOFEC performance.

3.2. Effect of operating temperature on CH₄-SOFEC

The effects of operating temperature on CH₄-SOFEC co-electrolysis and SOEC co-electrolysis of CO₂ and H₂O are shown in Fig. 4 and Fig.5. The detailed operation conditions are shown in Table 4.

As expected, the current density of both conventional SOEC for CO₂/H₂O co-electrolysis and CH₄-SOFEC for CO₂/H₂O co-electrolysis increase with increasing operation temperature (Fig.4a). Compared with conventional SOEC co-electrolysis, the performance of CH₄-SOFEC co-electrolysis has a much higher improvement with the increase of temperature. This advantage is mainly benefited from the quickly increase of SMR rate at higher temperature, which means more H₂ and CO can be converted from CH₄. Besides, from Fig. 4b it can be found that a higher temperature is beneficial to the performance improvement of CH₄-SOFEC in the whole range of applied cell potential. Especially when CH₄-SOFEC is operated at a high temperature, it can produce not only H₂ and CO at cathode but also electricity.

Fig. 5a shows the effect of temperature on the outlet gas composition in CH₄-SOFEC cathode. As the temperature is increased from 1023K to 1150K, the cathode outlet molar fractions for both H₂ and CO are increased, which is mainly due to the enhanced electrochemical reaction at a higher temperature. When temperature increases from 1150K to 1173K, the outlet molar fraction of CO is still increased but of the outlet molar fraction of H₂ is slightly decreased, which is caused by the favor for reversed WGSR at high temperature.

The gas composition change with temperature in anode is more complicated. In anode, methane reacts with H₂O to produces H₂ and CO and WGSR happens simultaneously. With the increase of temperature, the utilization ratio of methane is largely increased due to the higher SMR rate (Fig. 5b), which in turn results in a high outlet H₂ and CO concentration. It means that syngas

(CO and H₂ mixture) can be produced in both cathode and anode of CH₄-SOFEFC at a high temperature, offering an interesting way for effective syngas production.

From Fig. 6, we can see the difference of reversed WGS rate between different temperatures in cathode. When temperature is relatively low (1023K and 1073K), reversed WGS rate is relatively weak while when the temperature is high enough (1123K and 1173K), reversed WGS rate is very strong at the inlet part of cathode and then soon decreased to a level near 0 at the cathode outlet.

3.3. Effect of applied potential

The effects of operating voltage on conventional SOEC co-electrolysis of CO₂ and H₂O and CH₄-SOFEFC co-electrolysis of CO₂ and H₂O can also be seen from Fig.4.

As expected, the current density of both conventional SOEC for CO₂/H₂O co-electrolysis and CH₄-SOFEFC for CO₂/H₂O co-electrolysis increase with increasing operation potential (Fig. 4a). Compared with conventional SOEC co-electrolysis, CH₄-SOFEFC co-electrolysis operates at a much lower voltage to reach the same current density. When SOEC and CH₄-SOFEFC operates at a higher temperature, more electrical energy can be saved due to a much quicker SMR rate, which produces more H₂ and CO in anode.

3.4. Effect of inlet methane concentration

The effects of inlet methane concentration on CH₄-SOFEFC co-electrolysis of CO₂ and H₂O are shown in Fig. 7. The detailed operation conditions are shown in Table 5.

As shown in Fig. 7, the current density of CH₄-SOFEFC co-electrolysis of CO₂/H₂O increases with increasing methane concentration at 1073K. This behavior indicates that a higher inlet methane concentration can help save more electrical energy usage. This effect is more obvious when the applied voltage is higher as shown in Fig. 7. From Table 6 it can also be found that a

higher methane concentration can save much more electrical energy at higher current density. Corresponding with the effect on current density, cathode molar fraction of H₂ and CO also increases with higher anode inlet methane concentration as shown in Fig. 8. However, CH₄ is also a useful fuel for various applications. The optimal amount of CH₄ for CO₂/H₂O co-electrolysis needs to consider the energy/exergy efficiency as well as the economics of the system.

3.5. Effect of cathode inlet gas flow rate

The cathode inlet gas flow rate is varied to examine its effect on both SOEC co-electrolysis and CH₄-SOFEC co-electrolysis at different applied potentials and temperature. The cathode inlet gas flow rate changes from 20 SCCM to 200 SCCM with 1.3 V and 0.7 V applied voltage for SOEC and CH₄-SOFEC, respectively. More detailed operation conditions can be seen in Table. 7.

It can be found from Fig. 9a and Fig. 9b that the current density increases quickly with increasing cathode inlet gas flow rate in both SOEC and CH₄-SOFEC. This is because the higher flow rate of the H₂O/CO₂ mixture reduces the gas composition change along the gas channels and thus relatively higher reactant concentrations in the downstream, leading to better overall cell performance. However, the performance improvement is insignificant when the cathode gas flow rate is very high, as the gas composition along the gas channel becomes almost uniform.

3.6. Effect of anode inlet gas flow rate

The anode inlet gas flow rate is varied to examine its effect on both conventional SOEC co-electrolysis and CH₄-SOFEC co-electrolysis at different temperatures. The anode inlet gas flow rate changes from 20 SCCM to 100 SCCM at 1.4 V and 0.7 V applied voltage for SOEC and

CH₄-SOFEC, respectively. More detailed operation conditions can be seen in Table 8.

Fig. 10a shows the effect of anode inlet gas flow rate on SOEC current density change, at operating temperature of 1073 K. The SOEC performance is only slightly increased by about 1% with increasing anode flow rate from 20SCCM to 200 SCCM. In CH₄-SOFEC, the phenomenon is quite different as shown in Fig. 10b. With the increase of anode inlet gas flow rate in CH₄-SOFEC, its performance is increased with the anode gas flow rate is increased from 20 SCCM to about 50 SCCM but decreased gradually with further increase in anode flow rate at a temperature of 1123K. The existence of an optimal anode flow rate is mainly caused by the dependence of SMR rate on gas composition. With the increase of anode flow rate, more CH₄ and H₂O are supplied so that the amount of H₂ and CO produced through SMR is increased so that the performance of CH₄-SOFEC gets increased. However, if the anode flow rate is too large, the generated H₂ and CO are diluted by the CH₄/H₂O mixture, which in turn decreases the performance of CH₄-SOFEC. As SMR rate is much higher at a higher temperature, the decrease of CH₄-SOFEC performance at high anode flow rate is much slighter than that at lower temperature. Thus there exists a “best” anode flow rate at certain operation conditions, which can be determined.

4 Conclusions

A multi-physics model including electrochemical reaction, chemical reactions, ion/electronic charge transport, mass transport and momentum transport is developed to characterize the performance of a methane assisted SOEC for H₂O/CO₂ co-electrolysis. For comparison, a multi-physics model with same structure parameters is also developed to characterize the performance of an air assisted SOEC for H₂O/CO₂ co-electrolysis, which is validated by comparing the simulation results with experimental data offered by Shi's group.

It is found that the CH₄-assisting can significantly reduce the applied voltage thus greatly reduce

the electrical power consumption for H₂O/CO₂ co-electrolysis. At a low current density and sufficiently high temperature, the CH₄-SOFEC can be used for syngas and electrical power cogeneration.

The electrical power saving by CH₄-assisting can be increased by increasing the CH₄ concentration in the anode but the optimal amount of CH₄ concentration requires a full consideration of the energy/exergy efficiency and the economics of the CH₄-SOFEC system.

Another interesting finding is that the effect of anode gas flow rate is significant for CH₄-assisted SOEC. Optimal anode gas flow rate is observed for CH₄-assisted SOFEC. Regarding the cathode flow rate, the CH₄-SOFEC performance increases significantly with increasing cathode flow rate at the beginning but tends to approach a limit with further increase in the flow rate. This is totally different from the conventional SOEC in which the anode gas flow rate effect is small.

The present study also provides other detailed information for better understanding the working mechanism of methane assisted SOEC for H₂O/CO co-electrolysis like the important effect of WGSR in cathode.

Acknowledgement

This research was also supported by a grant of SFC/RGC Joint Research Scheme (X-PolyU/501/14) from Research Grant Council, University Grants Committee, Hong Kong SAR.

Nomenclature

Abbreviation

CH ₄ -SOFEC	Solid oxide CH ₄ -assisted electrolysis cell
F-T	Fischer Tropsch
LSM	Lanthanum strontium manganite
SMR	Steam methane reforming reaction
PEN	Positive Electrode-Electrolyte-Negative electrode assembly
SCCM	Standard cubic centime per minute
ScSZ	Scandium stabilized zirconium
SOEC	Solid oxide electrolysis cell
SOFEC	Solid oxide fuel-assisted electrolysis cell
TPB	Triple phase boundary
WGSR	Water gas shift reaction
YSZ	Yttrium stabilized zirconium

Roman

D_i^{eff}	Effective diffusivity of species i , $m^2 \cdot s^{-1}$
D_{ik}^{eff}	Knudsen diffusion coefficient of i , $m^2 \cdot s^{-1}$
D_{im}^{eff}	Molecular diffusion coefficient of i , $m^2 \cdot s^{-1}$
E	Equilibrium Nernst potential, V
E_a	Active energy, $J \cdot mol^{-1}$
F	Faraday constant, $96485 C \cdot mol^{-1}$
i_o	Exchange current density, $A \cdot m^{-2}$
k	Reaction rate constant, in terms of m , mol , Pa and s
K_{pr}, K_{ps}	Equilibrium constant of SMR and WGSR
n	Number of electrons transferred per electrochemical reaction
N_i	Flux of mass transport, $kg \cdot m^{-3} \cdot s^{-1}$
p	(partial) Pressure, Pa
R	Gas constant, $8.314 J \cdot mol^{-1} \cdot K^{-1}$
R_{MSR}	Rate of methane steam reforming reaction, $mol \cdot m^{-3} \cdot s^{-1}$
R_{WGSR}	Reaction rate of water gas shifting reaction, $mol \cdot m^{-3} \cdot s^{-1}$
T	Temperature, K
u	Velocity field, $m^3 \cdot s^{-1}$

Greek letters

α	Charge transfer coefficient
β_{H_2}	Electrochemical kinetics parameter for H ₂
ε	Porosity
κ	Permeability, m^2
ρ	Fluid density, $kg \cdot m^{-3}$
μ	Dynamic viscosity of fluid, $Pa \cdot s$
η_{act}	Anode activation polarization, V
η_{ohmic}	Ohmic polarization, V

Subscripts

an
ca

Anode
Cathode

Superscripts

0
L

Parameter at equilibrium conditions
Local

References

- [1] Ni M, Leung MKH, Leung DYC. Technological development of hydrogen production by solid oxide electrolyzer cell (SOEC). *Int J Hydrogen Energ.* 2008;33:2337-54.
- [2] Torrell M, Garcia-Rodriguez S, Morata A, Penelas G, Tarancon A. Co-electrolysis of steam and CO₂ in full-ceramic symmetrical SOECs: a strategy for avoiding the use of hydrogen as a safe gas. *Faraday Discussions.* 2015.
- [3] Ni M. Modeling of a solid oxide electrolysis cell for carbon dioxide electrolysis. *Chemical Engineering Journal.* 2010. 164(1): 246-254.
- [4] Graves C, Ebbesen SD, Mogensen M. Co-electrolysis of CO₂ and H₂O in solid oxide cells: Performance and durability. *Solid State Ionics.* 2011;192:398-403.
- [5] Ni M, Leung MKH, Leung DYC. A modeling study on concentration overpotentials of a reversible solid oxide fuel cell. *Journal of Power Sources.* 2006; 163(1): 460-466.
- [6] Ni M. 2D thermal modeling of a solid oxide electrolyzer cell (SOEC) for syngas production by H₂O/CO₂ co-electrolysis. *Int J Hydrogen Energ.* 2012;37:6389-99.
- [7] Wang Y, Liu T, Fang S, Xiao G, Wang H, Chen F. A novel clean and effective syngas production system based on partial oxidation of methane assisted solid oxide co-electrolysis process. *J Power Sources.* 2015;277:261-7.
- [8] Li W, Wang H, Shi Y, Cai N. Performance and methane production characteristics of H₂O–CO₂ co-electrolysis in solid oxide electrolysis cells. *Int J Hydrogen Energ.* 2013;38:11104-9.
- [9] Becker WL, Braun RJ, Penev M, Melaina M. Production of Fischer–Tropsch liquid fuels from high temperature solid oxide co-electrolysis units. *Energy.* 2012;47:99-115.
- [10] Chen B, Xu H, Chen L, Li Y, Xia C, Ni M. Modelling of One-Step Methanation Process Combining SOECs and Fischer-Tropsch-like Reactor. *J Electrochem Soc.* 2016;163:F3001-F8.
- [11] Cinti G, Baldinelli A, Di Michele A, Desideri U. Integration of Solid Oxide Electrolyzer and Fischer-Tropsch: A sustainable pathway for synthetic fuel. *Applied Energy.* 2016;162:308-20.
- [12] Stempien JP, Ni M, Sun Q, Chan SH. Thermodynamic analysis of combined Solid Oxide Electrolyzer and Fischer–Tropsch processes. *Energy.* 2015;81:682-90.
- [13] Chen L, Chen F, Xia C. Direct synthesis of methane from CO₂-H₂O co-electrolysis in tubular solid oxide electrolysis cells. *Energy & Environmental Science.* 2014;7:4018-22.
- [14] Luo Y, Shi Y, Li W, Ni M, Cai N. Elementary reaction modeling and experimental characterization of solid oxide fuel-assisted steam electrolysis cells. *Int J Hydrogen Energ.* 2014;39:10359-73.
- [15] Stempien JP, Liu Q, Ni M, Sun Q, Chan SH. Physical principles for the calculation of equilibrium potential for co-electrolysis of steam and carbon dioxide in a Solid Oxide Electrolyzer Cell (SOEC). *Electrochimica Acta.* 2014;147:490-7.
- [16] Luo Y, Shi Y, Li W, Cai N. Comprehensive modeling of tubular solid oxide electrolysis cell for co-electrolysis of steam and carbon dioxide. *Energy.* 2014;70:420-34.
- [17] Ni M. An electrochemical model for syngas production by co-electrolysis of H₂O and CO₂. *J Power Sources.* 2012;202:209-16.
- [18] Costamagna P, Honegger K. Modeling of Solid Oxide Heat Exchanger Integrated Stacks and Simulation at High Fuel Utilization. *J Electrochem Soc.* 1998;145:3995-4007.
- [19] Ni M. Modeling of SOFC running on partially pre-reformed gas mixture. *Int J Hydrogen Energ.* 2012;37:1731-45.
- [20] Suwanwarangkul R, Croiset E, Fowler MW, Douglas PL, Entchev E, Douglas MA. Performance comparison of Fick's, dusty-gas and Stefan–Maxwell models to predict the concentration overpotential of a SOFC anode. *J Power Sources.* 2003;122:9-18.

- [21] Chan SH, Khor KA, Xia ZT. A complete polarization model of a solid oxide fuel cell and its sensitivity to the change of cell component thickness. *J Power Sources*. 2001;93:130-40.
- [22] Lehnert W, Meusinger J, Thom F. Modelling of gas transport phenomena in SOFC anodes. *J Power Sources*. 2000;87:57-63.
- [23] Luo Y, Shi Y, Li W, Cai N. Dynamic electro-thermal modeling of co-electrolysis of steam and carbon dioxide in a tubular solid oxide electrolysis cell. *Energy*. 2015.

Tables

Table.1 Model parameters[16]

Parameters	Value or expression	Unit
Ionic conductivity		
ScSZ	$6.92 \times 10^4 \exp(-9681/T)$	Sm^{-1}
YSZ	$3.34 \times 10^4 \exp(-10300/T)$	Sm^{-1}
Electronic conductivity		
LSM	$4.2 \times 10^7 \exp(-1150/T)$	Sm^{-1}
Ni	$4.2 \times 10^6 - 1065.3T$	Sm^{-1}
Porosity		
Cathode support layer	0.36	
Cathode active layer	0.36	
Anode	0.36	
S_{TPB}		
Cathode layer	2.14×10^5	m^2m^{-3}
Anode layer	2.14×10^5	m^2m^{-3}

Table. 2 Operation parameters for model validation

Parameter	Value	Unit
Anode gas flow rate	150	SCCM
Cathode gas flow rate	350	SCCM
Anode gas composition	Air	
Cathode gas composition	CO ₂ (28.6%)+H ₂ O(28.6%)+H ₂ (14.3%)+N ₂ (28.5%)	
Temperature	1073	K

Table.3 Model tuning parameters

Parameter	Value	Unit
Cathode tortuosity	3	
Anode tortuosity	3	
H₂ electrochemical kinetics, β_{H_2}	3.3×10^8	Am^{-2}
O₂ electrochemical kinetics, β_{O_2}	4.2×10^7	Am^{-2}
H₂ charge transfer coefficient, α_{H_2}	0.65	
CO charge transfer coefficient, α_{CO}	0.65	
O₂ charge transfer coefficient, α_{O_2}	0.5	

Table.4 Operation parameters for temperature effect study

Parameter	SOFEC	SOEC	Unit
Anode flow rate	100	100	SCCM
Cathode flow rate	100	100	SCCM
Anode gas composition	40%CH ₄ &H ₂ O+20%N ₂	Air	
Cathode gas composition	40%CO ₂ &H ₂ O+20%N ₂	40%CO ₂ &H ₂ O+20%N ₂	
Temperature	1023, 1073, 1123	1023, 1073, 1123	K

Table.5 Operation parameters for inlet methane concentration effect study

Parameter	SOFEC	Unit
Anode flow rate	100	SCCM
Cathode flow rate	100	SCCM
Anode gas composition	40%CH ₄ &H ₂ O+20%N ₂ ; 30%CH ₄ &H ₂ O+40%N ₂ ; 20%CH ₄ &H ₂ O+60%N ₂ ;	
Cathode gas composition	40%CO ₂ &H ₂ O+20%N ₂	
Temperature	1073	K

Table.6 Comparison of applied voltage between different inlet methane concentrations

	40%CH4- SOFEC	20%CH4- SOFEC	
Current density (A/m²)	Applied voltage (V)		Electricity energy save (W/m²)
400	0.1	0.15	20, (33%)
800	0.16	0.24	64, (33%)
1200	0.21	0.31	120, (32%)
1600	0.25	0.39	224, (36%)
2000	0.28	0.47	380, (40%)

Table.7 Operation parameters for cathode inlet gas flow rate effect study

Parameter	SOFEC	SOEC	Unit
Anode gas flow rate	100	100	SCCM
Anode gas composition	40%CH ₄ &H ₂ O+20%N ₂	Air	
Cathode gas composition	CO ₂ (40%)+H ₂ O(40%)+N ₂ (20%)	CO ₂ (40%)+H ₂ O(40%)+N ₂ (20%)	
Temperature	1073, 1123	1023	K
Applied voltage	0.7	1.4	V

Table.8 Operation parameters for anode inlet gas flow rate effect study

Parameter	SOFEC	SOEC	Unit
Cathode gas flow rate	100	100	
Anode gas composition	40%CH ₄ &H ₂ O+20%N ₂	Air	
Cathode gas composition	CO ₂ (40%)+H ₂ O(40%)+N ₂ (20%)	CO ₂ (40%)+H ₂ O(40%)+N ₂ (20%)	
Temperature	1073, 1123	1073	K
Applied voltage	0.7	1.4	V

List of Figures

Fig.1 Schematic of traditional SOEC

Fig.2 Schematic of CH₄-assisted SOFEC

Fig.3 Comparison of calculated data with experimental data for model validation

Fig.4 Effect of temperature on CH₄-SOFEC and SOFC co-electrolysis: (a) at 0.7V and 1.4V for CH₄-SOFEC and SOEC, respectively (b) at operating temperature of 1023K, 1073K and 1123K for CH₄-SOFEC and SOEC

Fig.5 Effect of temperature on the outlet gas composition in (a) CH₄-SOFEC cathode and (b) CH₄-SOFEC anode at operating voltage of 0.7V

Fig.6 WGS rate (vertical axis, mol m⁻³ s⁻¹) at different temperatures in cathode

Fig.7 Effects of inlet methane mole fraction on CH₄-SOFEC performance at 1073K

Fig.8 Distribution of H₂ and CO mole fractions in cathode at 20% (a, d), 30% (b, e), 40% (c, f) inlet methane mole fraction at applied voltage of 0.7V and temperature of 1073K

Fig.9 Effects of cathode inlet gas flow rate on the performance of (a) CH₄-SOFEC at 0.7V and (b) SOEC at 1.4V

Fig.10 Effects of anode inlet gas flow rate on (a) SOEC and (b) CH₄-SOFEC performance at 1.4 V and 0.7V applied voltage, respectively

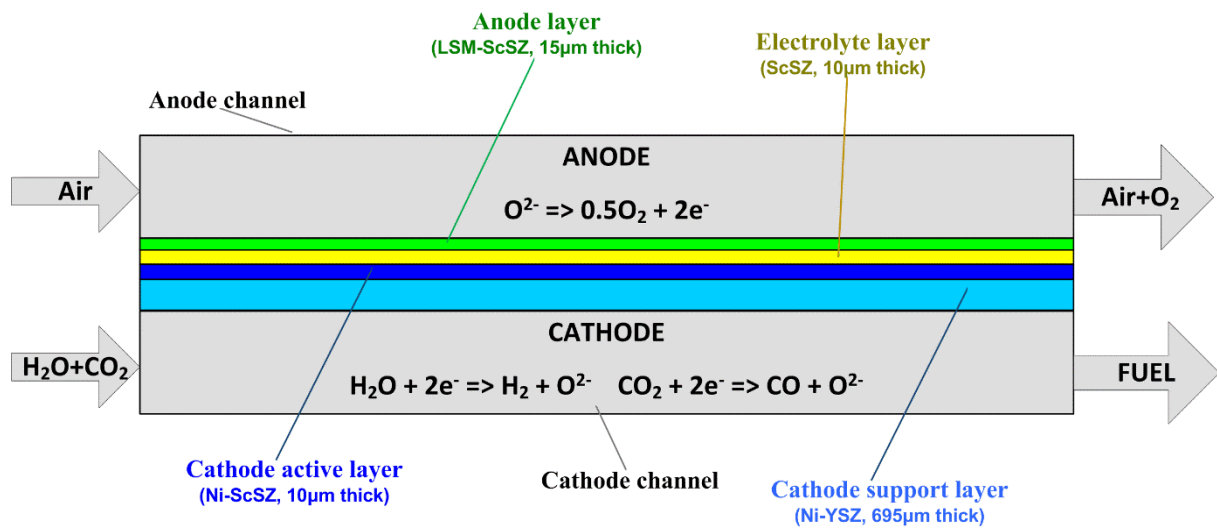


Fig.1 Schematic of traditional SOEC

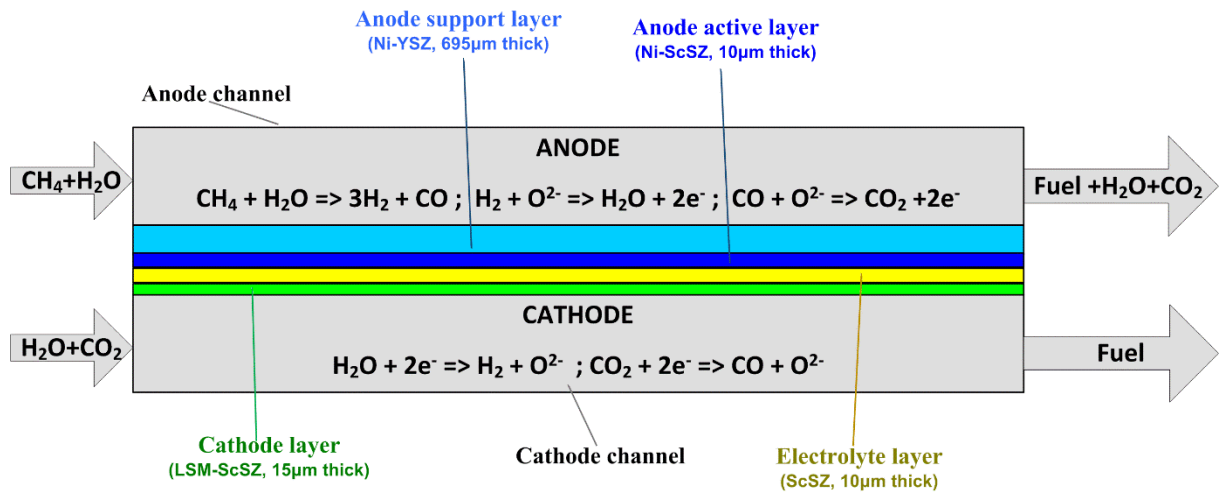


Fig.2 Schematic of CH₄-assisted SOFEC

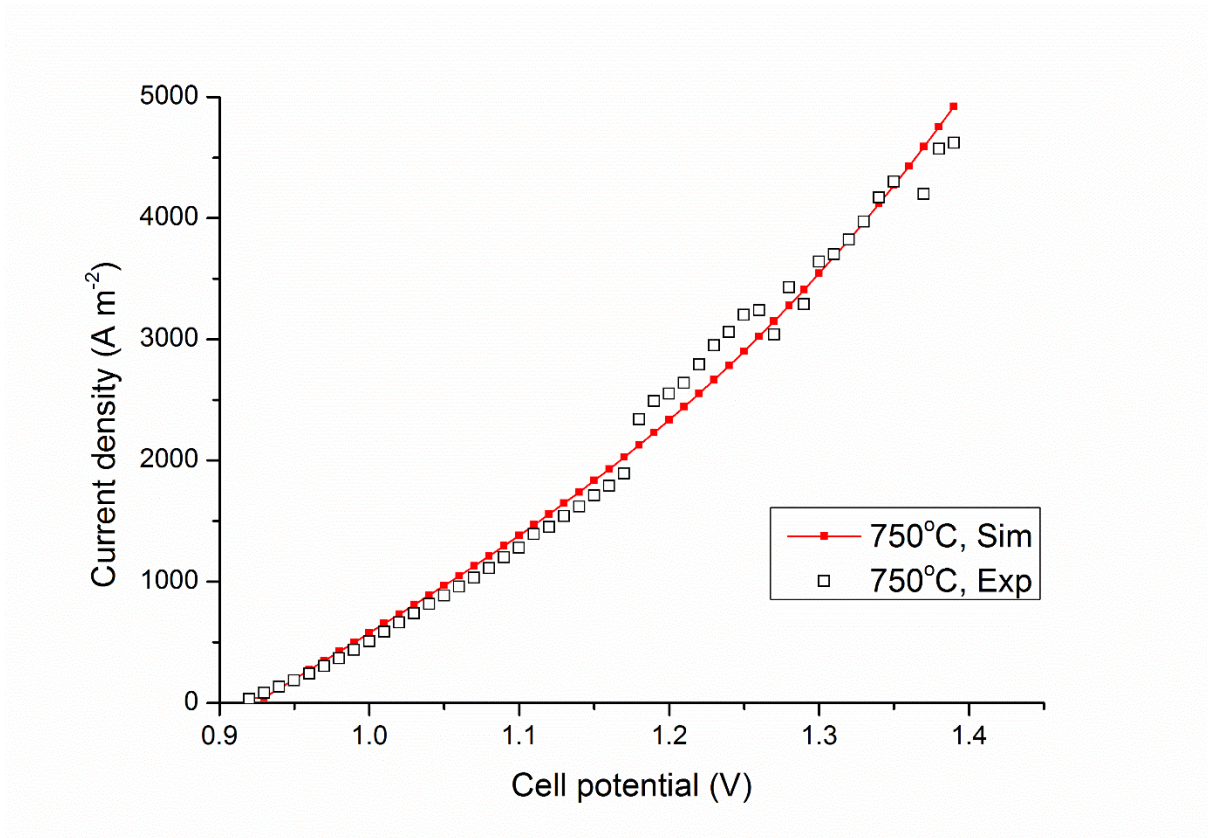


Fig.3 Comparison of calculated data with experimental data for model validation

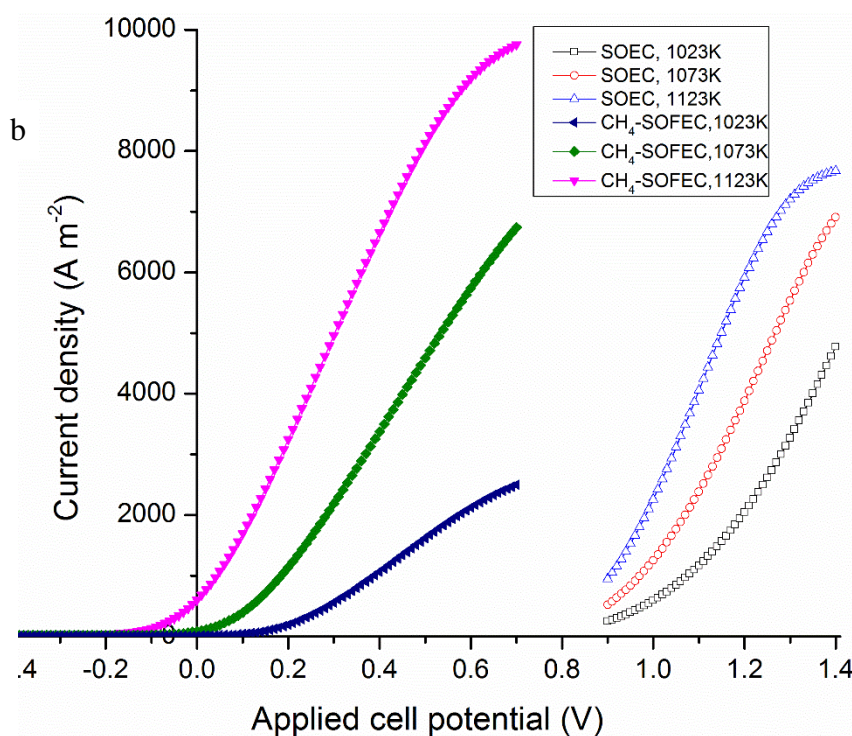
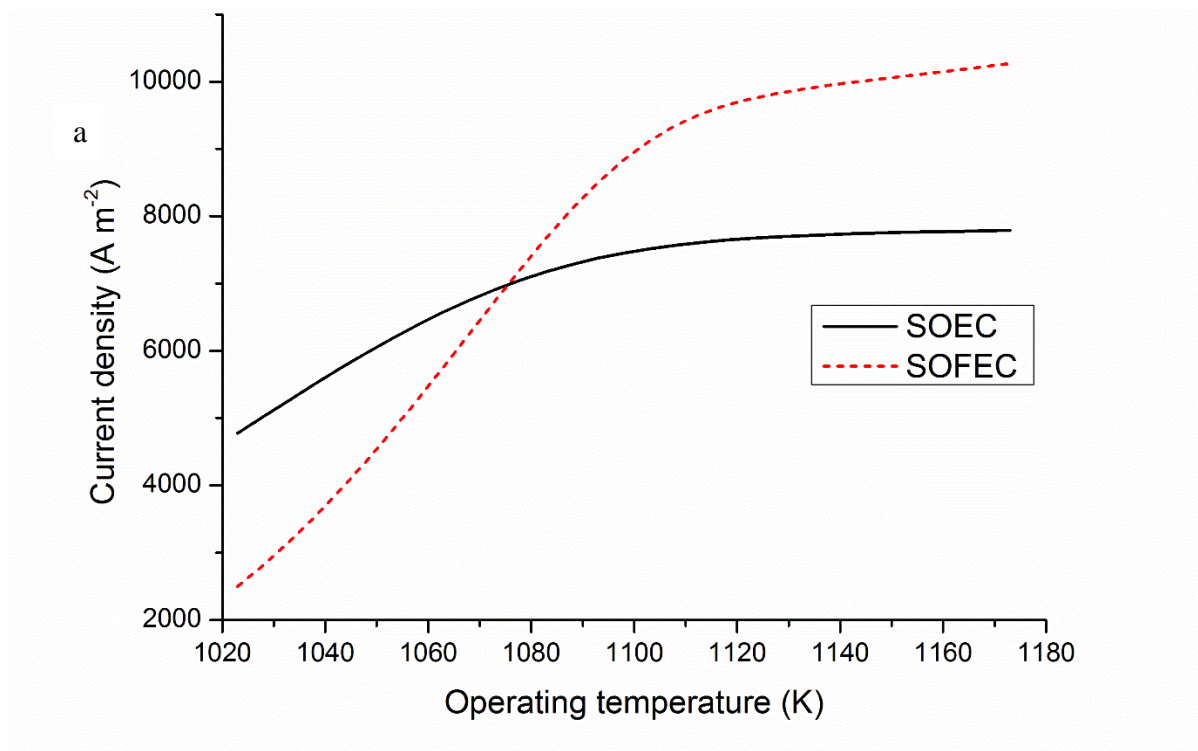


Fig.4 Effect of temperature on CH_4 -SOFEC and SOFC co-electrolysis: (a) at 0.7V and 1.4V for CH_4 -SOFEC and SOEC, respectively (b) at operating temperature of 1023K, 1073K and 1123K for CH_4 -SOFEC and SOEC.

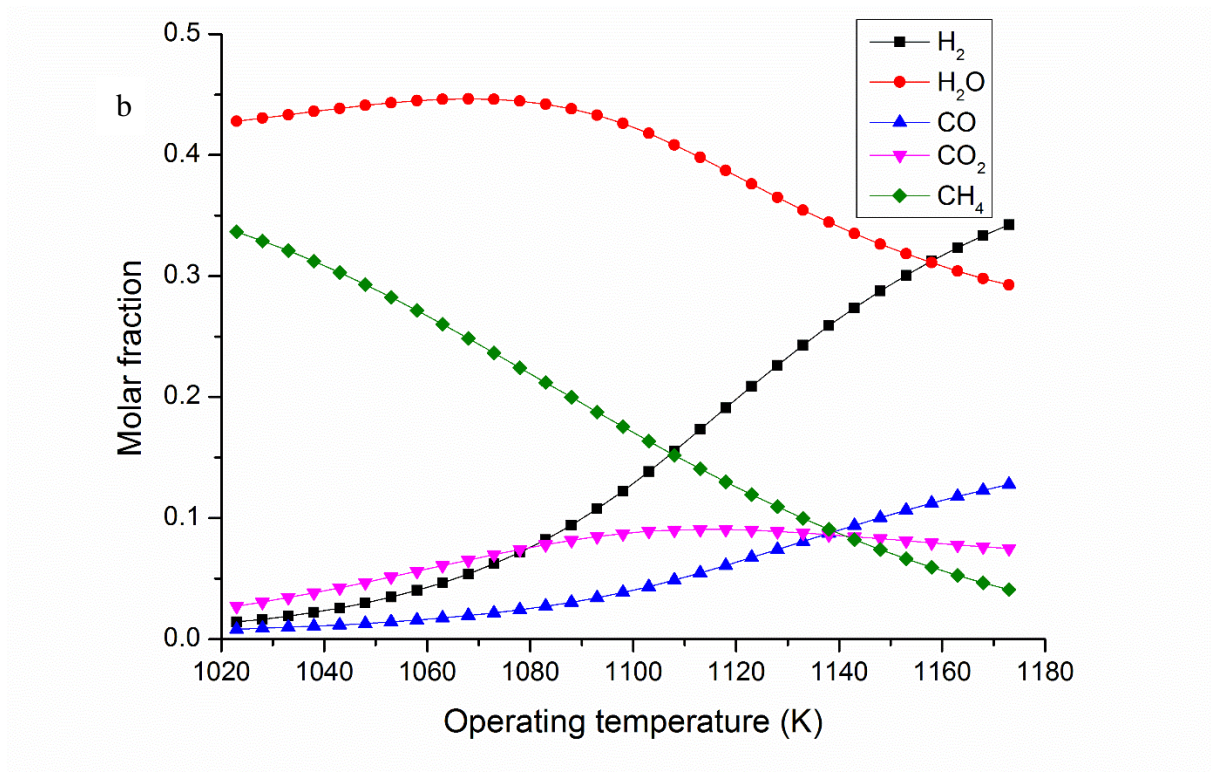
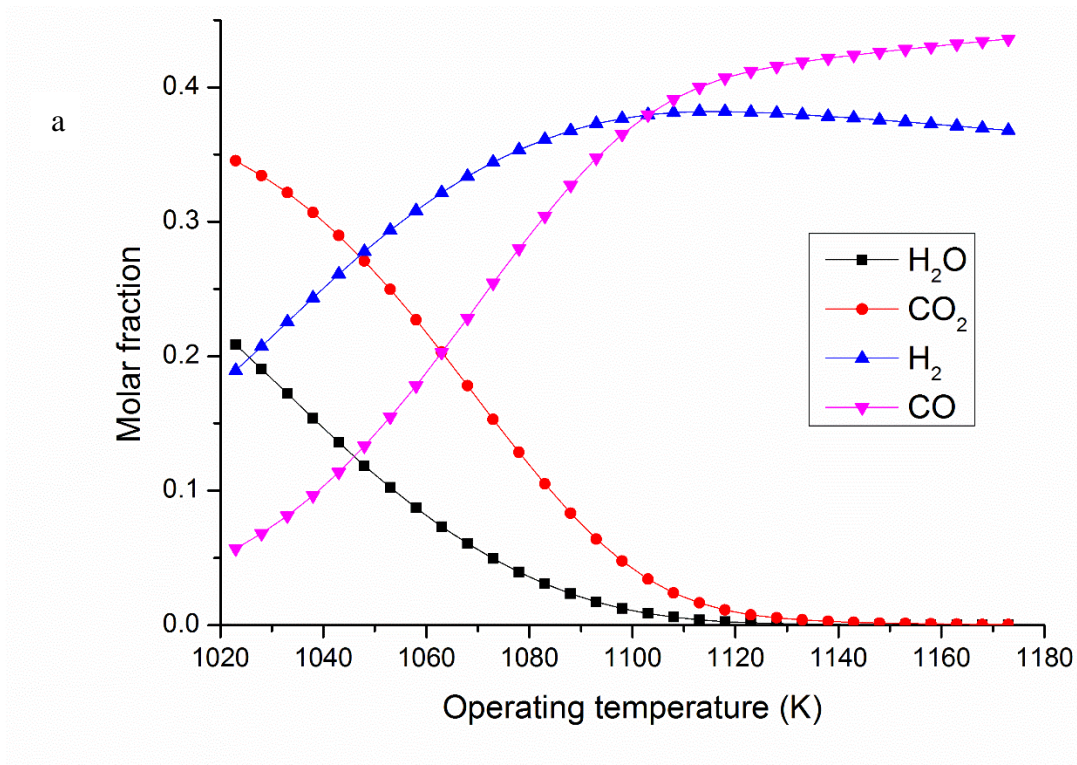


Fig.5 Effect of temperature on the outlet gas composition in (a) CH₄-SOFEC cathode and (b) CH₄-SOFEC anode at operating voltage of 0.7V.

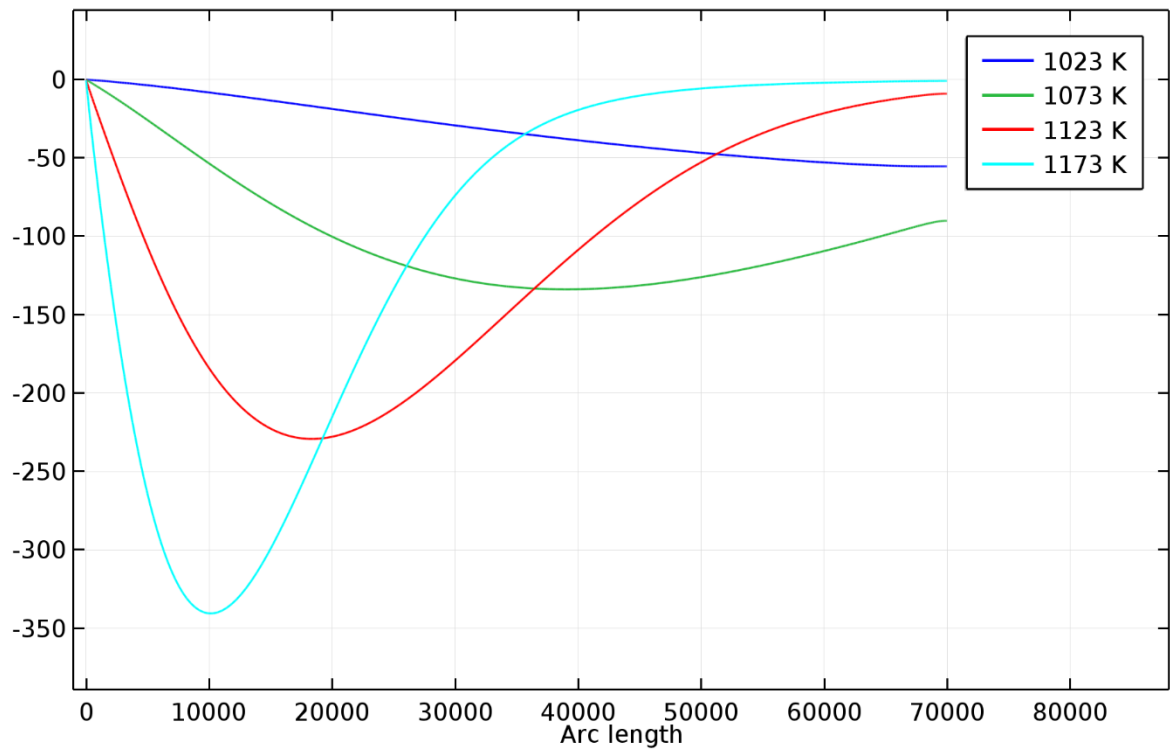


Fig.6 WGSR rate (vertical axis, mol m⁻³ s⁻¹) at different temperatures in cathode

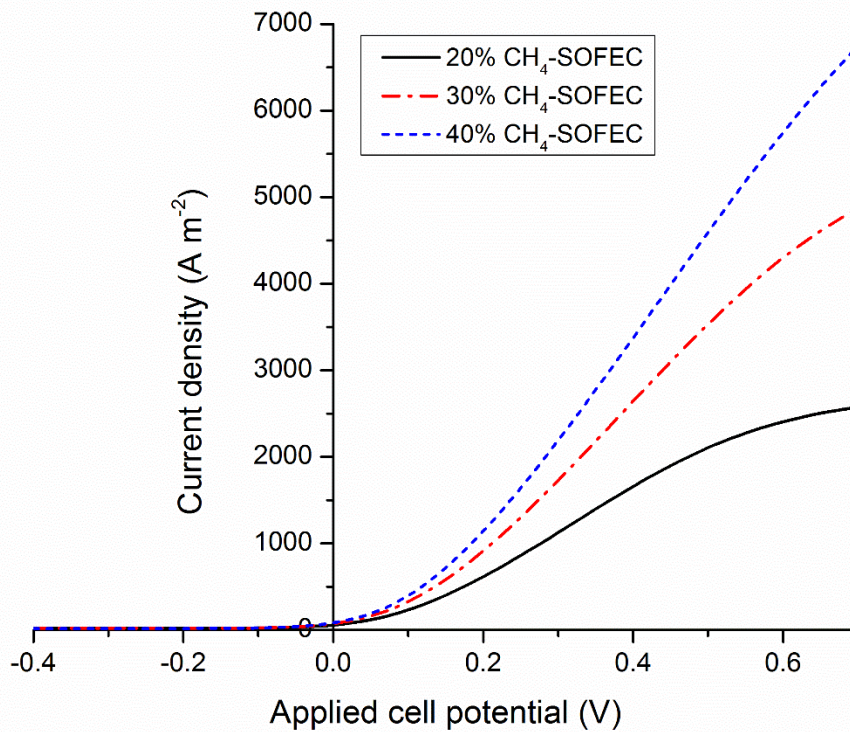


Fig.7 Effects of inlet methane mole fraction on CH₄-SOFEC performance at 1073K.

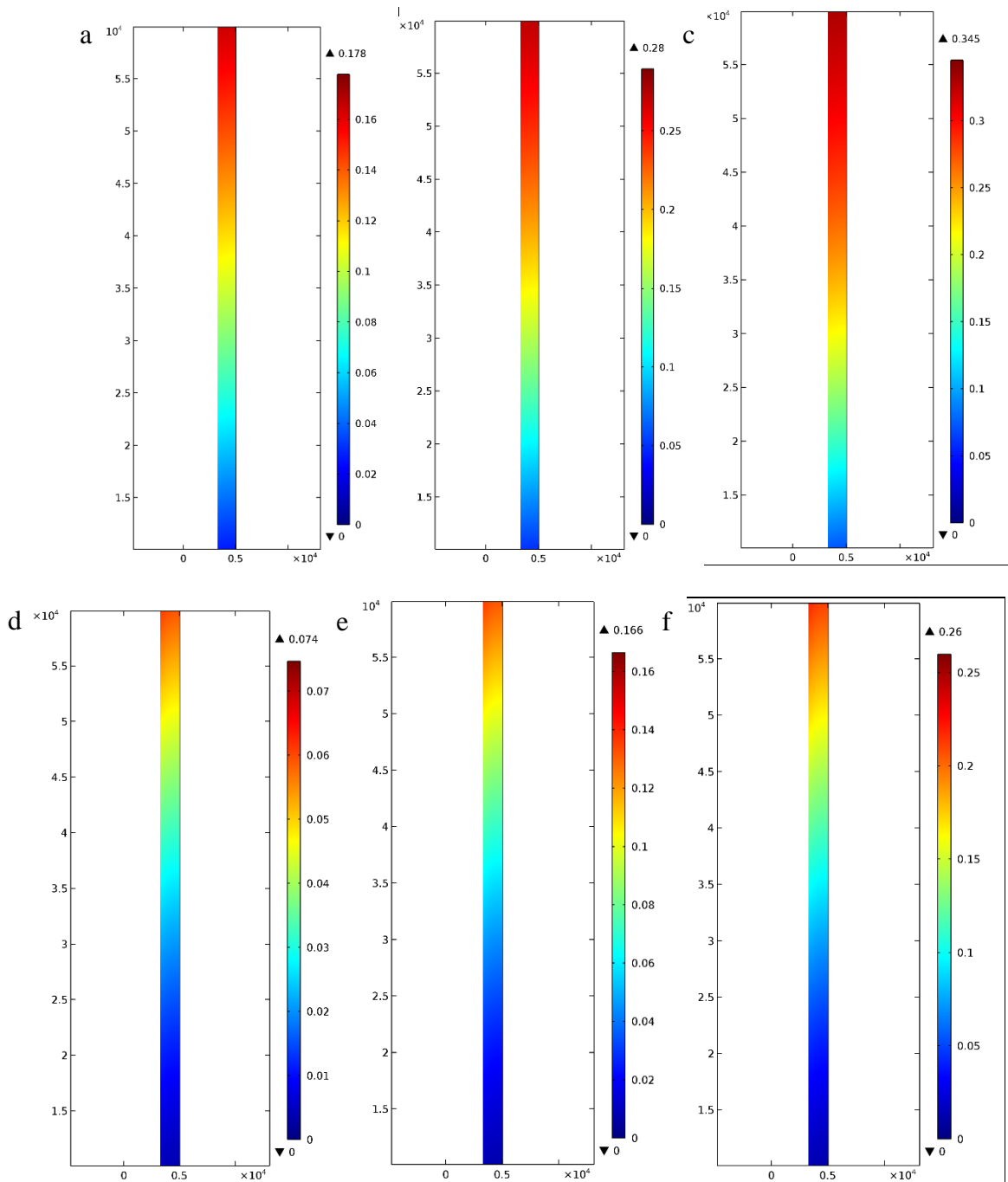


Fig.8 Distribution of H₂ and CO mole fractions in cathode at 20% (a, d), 30% (b, e), 40% (c, f) inlet methane mole fraction at applied voltage of 0.7V and temperature of 1073K

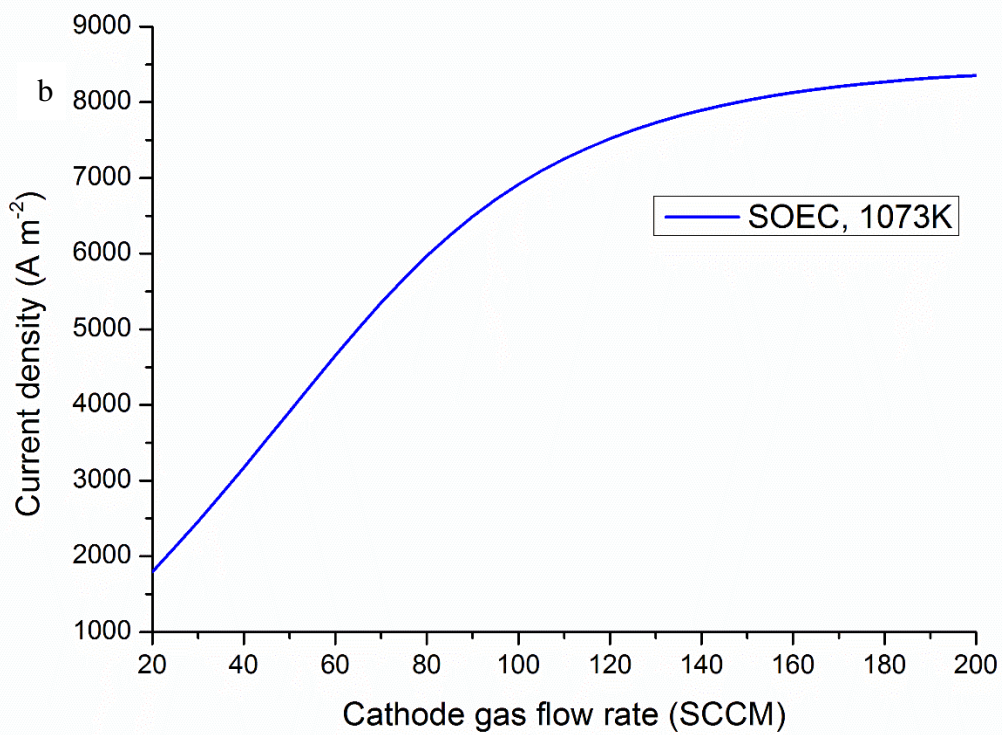
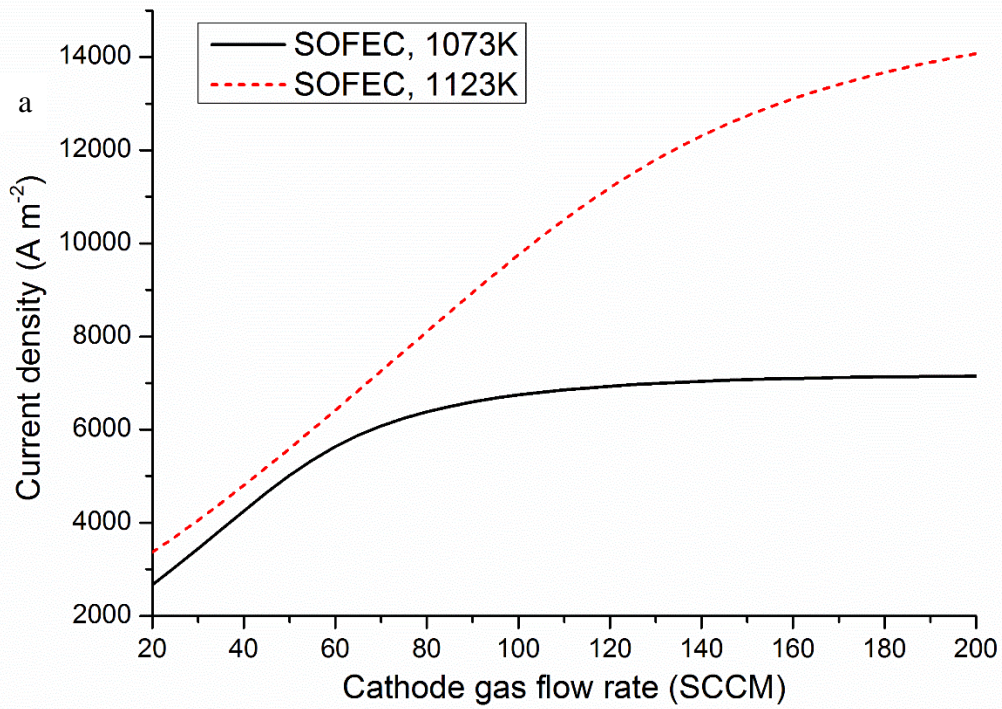


Fig.9 Effects of cathode inlet gas flow rate on the performance of (a) CH₄-SOFEC at 0.7V and (b) SOEC at 1.4V.

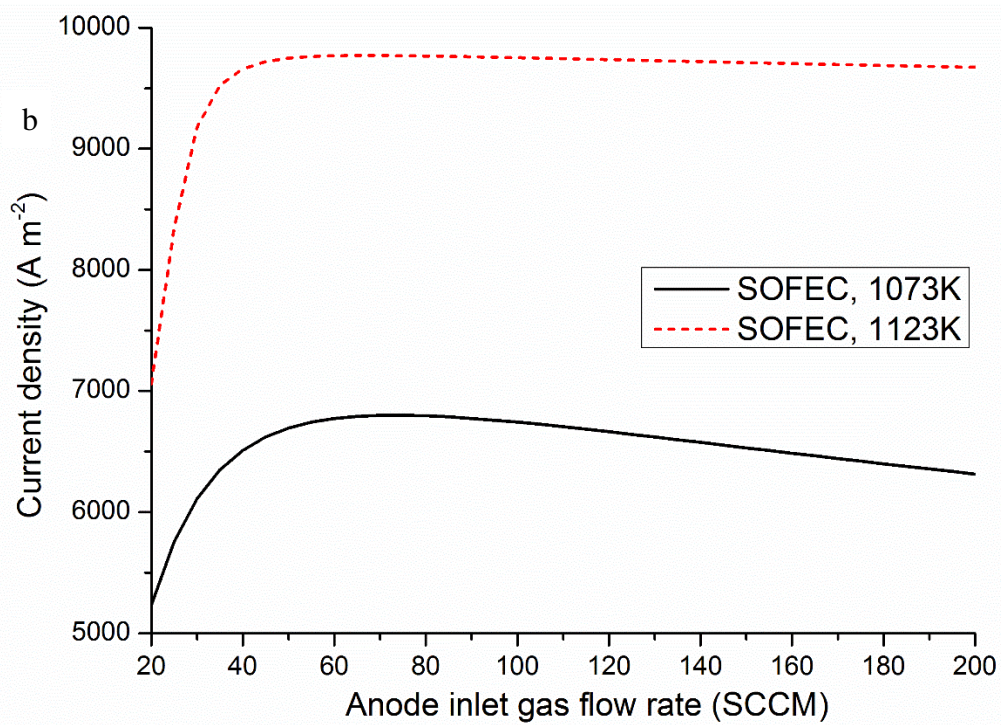
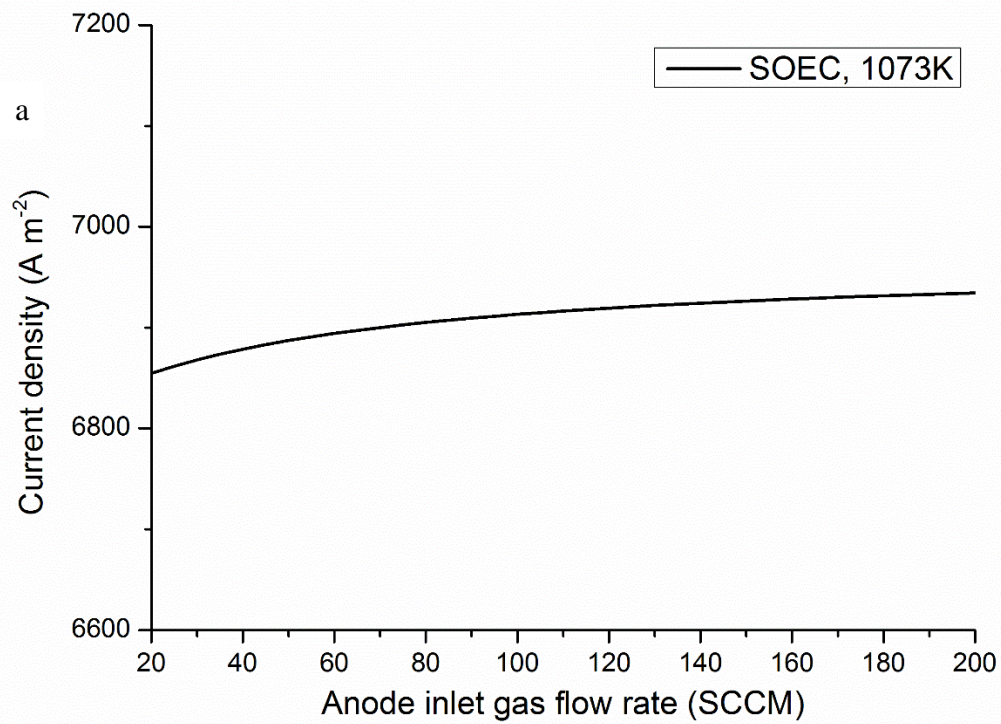


Fig.10 Effects of anode inlet gas flow rate on (a) SOEC and (b) CH₄-SOFEC performance at 1.4 V and 0.7V applied voltage, respectively.